JACS
JOURNAL OF THE AMERICAN CHEMICAL SOCIETY
pubs.acs.org/JACS
Article

Enhanced Menshutkin S_N2 Reactivity in Mesoporous Silica: The Influence of Surface Catalysis and Confinement

Weizhong Zheng,[§] Steven A. Yamada,[§] Samantha T. Hung, Weizhen Sun, Ling Zhao,* and Michael D. Fayer*

Cite This: https://dx.doi.org/10.1021/jacs.9b12666
Read Online
ACCESS | Metrics & More | Article Recommendations | Supporting Information

ABSTRACT: A significant enhancement in the Menshutkin S_N2 reaction between 1-methylimidazole (MeIm) and methyl thiocyanate (MeSCN) is observed when the reaction is confined in the nanoscale silica pores of MCM41 and SBA15. The experiments in the silica pores are conducted without the surrounding bulk reaction mixture. The influences of temperature, pore radius, and surface chemistry on the kinetics of the confined reaction are analyzed with time-dependent infrared spectroscopy, molecular dynamics simulations, and ab initio calculations. The rate constant of the pseudo-first order reaction increases with decreasing pore size, and the activation energy is found to decrease by 5.6 kJ/mol in the smallest pore studied (2.8 nm) relative to the bulk reaction. The rate constant dependence on pore size is accurately described by a two-state model in which molecules within the 4.6 Å interfacial layer experience a 2.4-fold rate constant increase relative to those reacting at the bulk rate further away from the interface. The removal of polar silanol groups from the silica surface via passivation with trimethylsilyl chloride results in bulk-like kinetics despite a reduction in the pore diameter, demonstrating the role of silanols as catalytic sites. Electronic structure calculations of the energy profile on a model silica surface confirm that silanol groups, particularly those of the vicinal type, can reduce the activation energy and reaction endothermicity through the donation of hydrogen bonds to the reactant, transition state, and product complexes.

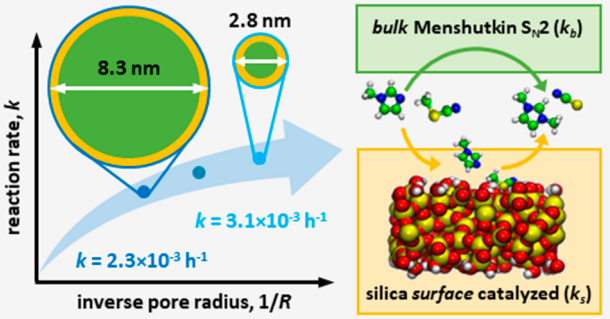

1. INTRODUCTION

The energy profile of a chemical reaction can change dramatically when it is confined in a nanostructure.[1−3] Hence, confinement is being increasingly explored as a strategy to promote and control reactions. Reaction kinetics can be enhanced when interactions between guest molecules and the interface arrange them in a preferential configuration for reaction, stabilize the transition state, or promote increased local reactant concentrations.[2,3] If multiple products are possible, changes in the relative stabilities of their transition states can alter selectivity.[4] These effects have been mainly studied through simulation by comparing calculated energy profiles in model nanostructures, such as carbon nanotubes (CNTs), to those in the gas phase.[5−8] In contrast, few experimental studies have selectively probed the kinetics of nanoconfined reactions, making the evaluation of models difficult.

Of the many reactions of interest, the Menshutkin S_N2 reaction[9] is notable for its use in the study of solvent and medium effects on chemical reactivity.[10−14] This special class of S_N2 reactions involves the alkylation of a formally sp^2 or sp^3 hybridized nitrogen atom[12]

$$Nu + RL \rightarrow NuR^+ + L^- \quad (1)$$

where Nu and L represent the nucleophile (amine) and leaving group, respectively. The nucleophilic attack occurs on the opposite side of the substrate (RL) relative to the leaving group, resulting in the typical S_N2 transition state consisting of a 5-coordinated carbon atom.[13] Since the reaction involves the formation of ionic products from neutral reactants, it is heavily influenced by the nature of the solvent, and large increases in the reaction rate have been observed with increases in solvent polarity and polarizability.[10−13]

Recently, calculated energy profiles for the Menshutkin reaction between NH_3 and CH_3Cl showed that the polarizable surface of CNTs stabilizes charge separation over the course of the reaction, implying a rate enhancement for the confined reaction.[5,8,15] In contrast, the energy barrier for the conventional S_N2 reaction between Cl^- and CH_3Cl was found to increase in CNTs.[6,7] The increased barrier was attributed to

Received: November 24, 2019
Published: February 20, 2020

destabilizing C−H···π interactions between the transition state and electron cloud of the CNT surface. These results indicate that, depending on the nature of the reaction, the same nanostructure property can induce opposing effects on reactivity. However, these predictions remain challenging to verify owing to heterogeneity and impurities in CNT structures,[8,16] difficulty in encapsulating reactants,[3] and a lack of well-defined probes of confined kinetics.

The uniform and tunable (~2−50 nm diameter) cylindrical pores of mesoporous silica[17,18] offer a well-defined medium for studying confined reactions. Although these materials are typically used as catalyst supports, the pure forms exhibit complex activity in certain reactions.[19−21] The mesoporous silica MCM41 was found to be an effective catalyst for the acetalization of cyclohexanone with methanol.[19] The rate initially increased with decreasing pore diameter until a maximum was obtained at ~1.9 nm, with further pore size reductions decreasing the rate.[19] Similarly, yields for the intramolecular cyclization of *N*-phenylanthranilic acid increased significantly with decreasing pore diameter,[20] and the material was later shown to be an effective catalyst for the synthesis of α-aminonitriles and imines in the Strecker reaction.[21] However, because the silica was mixed with the bulk reaction mixtures in the above cases, the kinetics did not exclusively reflect those of the confined volume. For example, the diffusion of reactants and products in and out of the pores can strongly influence the observed rates.[22]

In the present work, the influence of surface catalysis and confinement on reaction kinetics is studied by observing a Menshutkin reaction in mesoporous silica (Figure 1). Care was

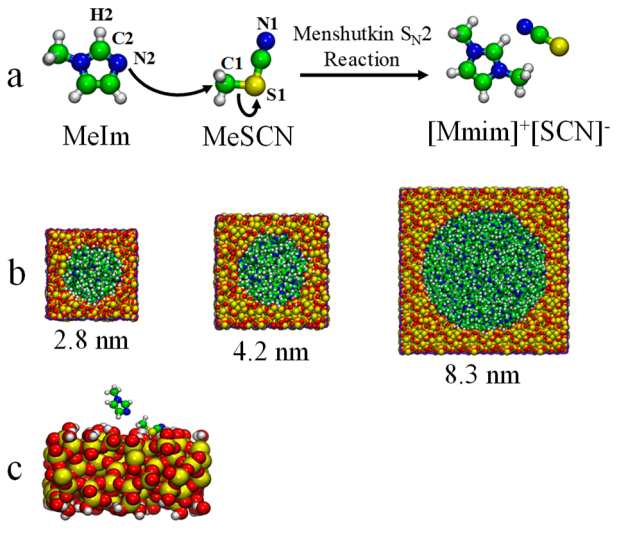

Figure 1. (a) Optimized molecular structures of MeIm, MeSCN, and $[Mmim]^+[SCN]^-$ with atom labels, and the corresponding reaction pathway. (b) MD simulation snapshots of the MeIm and MeSCN confined in the silica pore models of different size. (c) Silica surface model for the electronic structure calculations.

taken to fully condense the reactants, 1-methylimidazole (MeIm, nucleophile) and methyl thiocyanate (MeSCN, substrate; Figure 1a), in the pores (Figure 1b) and eliminate all external bulk reaction mixture. In this reaction, the nucleophilic N2 atom of MeIm attacks the electrophilic C1 of MeSCN, leading to the loss of the SCN^- leaving group (Figure 1a). The carbon bonded to the two nitrogen atoms of MeIm is referred to as C2. The results are compared to the same reaction in bulk solution. The concentration of the SCN^- leaving group is monitored in real-time with Fourier transform infrared (FT IR) spectroscopy, yielding pseudo-first order rate constants for the reaction. The temperature dependence of the rate constant in the smallest pore studied (2.8 nm) is contrasted with that in bulk solution, showing that the pore reduces the activation energy barrier by 5.6 kJ/mol.

The rate constants increase as the pore diameter decreases in the order 8.3, 4.2, and 2.8 nm. The trend is quantitatively described by a two-state model in which molecules within the surface layer experience a 2.4-fold rate constant increase over those reacting at the bulk rate in the pore interior. Chemical passivation of polar silanol groups on the surface deactivates the catalytic activity of the silica, implicating silanols in the rate constant enhancement. Electronic structure calculations on a model silica surface (Figure 1c) confirm that silanol groups, particularly vicinal ones, donate hydrogen bonds to key complexes over the course of the reaction, reducing the activation energy barrier and reaction endothermicity.

2. EXPERIMENTAL PROCEDURES

2.1. Sample Characterization, Preparation, and Measurement. The BET surface areas,[23] BJH pore diameter distributions,[24] and pore volumes of the investigated mesoporous silica samples (Table 1) were characterized with N_2 (g) sorption isotherms taken at the Soft & Hybrid Materials Facility (SMF) at the Stanford Nano Shared Facilities (SNSF).

Table 1. Surface Areas, Pore Diameters, and Total Pore Volumes of Mesoporous Silica Samples

materials	S_{BET} (m^2/g)	pore diameter (nm)	V_t (cm^3/g)
SBA15	520 ± 60	8.3 ± 0.1	1.50 ± 0.10
SBA15	560 ± 80	4.2 ± 0.5	0.62 ± 0.06
MCM41	950 ± 70	2.8 ± 0.1	0.82 ± 0.05
MCM41-Si(Me)$_3$	621 ± 15	2.3 ± 0.1	0.51 ± 0.01

Representative sorption isotherms and pore diameter distributions can be found in the Supporting Information, SI. The hydroxyl groups on the pore surface of the 2.8 nm MCM41 sample were replaced with $Si(Me)_3$ groups as previously described to yield the MCM41-$Si(Me)_3$ sample.[25−27] The synthetic procedure and FT IR spectrum of the passivated material are detailed in the SI.

The 1:10 MeSCN:MeIm reaction mixture was confined in the porous materials by mixing them with the solution, filtering the particles, and equilibrating them in a home-built flow chamber to ensure that excess bulk solution was removed while fully filling the pores. The detailed procedure is described in the SI. The percent mass losses from the materials subjected to thermogravimetric analysis (TGA) were consistent with the measured pore volumes, confirming the reliability of the method.[28]

The silica samples containing the confined Menshutkin reaction were assembled in a sample cell as previously described.[28] FT IR spectra were acquired every 30 min for the initial 20 h of the reaction. The sample was then heated up to 356.2 K and the spectra were taken until the reaction was complete. The fractional yield of SCN^- over the course of the reaction was computed from the time-dependent spectrum of the CN stretch mode as discussed in the SI.

3. RESULTS AND DISCUSSION

3.1. Linear IR Spectrum. In Figure 2, the normalized, background subtracted CN stretch vibrations of the MeSCN (Figure 2a) and SCN^- (Figure 2b) in bulk and confined MeIm are compared. The physical characteristics of the pores used in this study are given in Table 1. The band centers and line

https://dx.doi.org/10.1021/jacs.9b12666
J. Am. Chem. Soc. XXXX, XXX, XXX−XXX

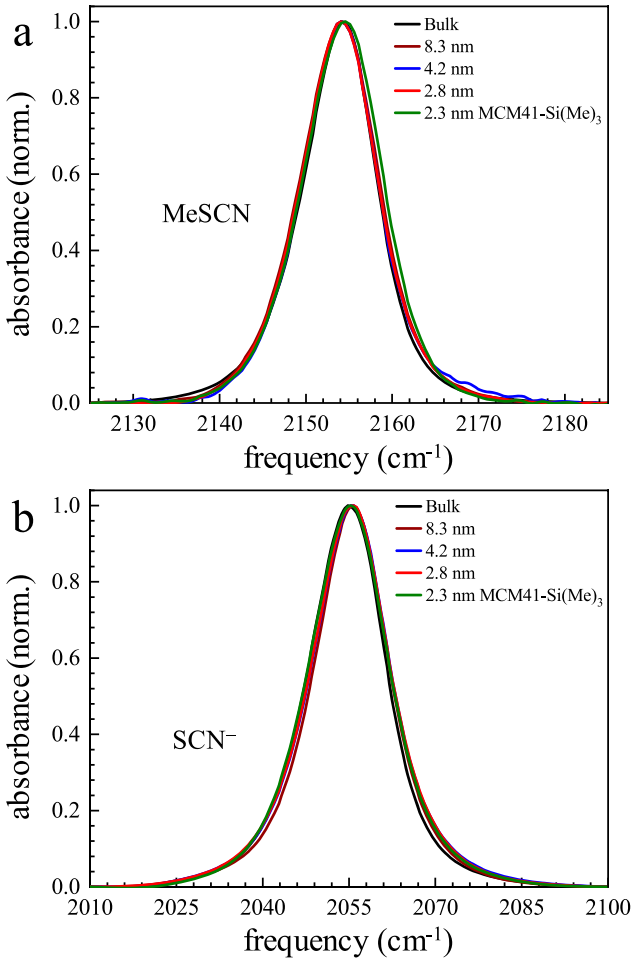

Figure 2. Normalized, background subtracted FT IR spectra of the CN stretch mode of (a) MeSCN and (b) SCN^- in bulk MeIm (black curve) and in MeIm confined in the unpassivated 8.3 (brown curve), 4.2 (blue curve), 2.8 (red curve), and passivated 2.3 nm (green curve) silica pores.

widths are listed in Table 2. Nanoscale confinement has little influence on the peak center of MeSCN, which is 2154 cm^{-1} in every pore system. However, the full width at half-maximum of the confined line shape is slightly broadened compared to that of the bulk line shape. This slight broadening likely results from the formation of hydrogen bonds (H-bonds) between the CN and silanol groups on the pore wall for a small fraction of the MeSCN molecules, leading to a broader range of transition frequencies.[29] The CN can accept an H-bond from the mildly positive H2 of MeIm (Figure 1a),[30] but this interaction is substantially weaker than the acceptance of an H-bond from the surface silanols. The additional H-bonds formed with the silica surface lead to greater inhomogeneous broadening of the spectrum relative to that in the bulk liquid. The increased width on the blue side is consistent with the blue-shift observed for the CN stretch of acetonitrile confined in mesoporous silica, which was attributed to hydrogen bonding between the CN and OH groups on the pore surface.[31] In the case of SCN^-, the peak center blue shifts very slightly upon nanoscale confinement (Table 2), which is also consistent with the observations for acetonitrile.[31] It was previously found that axial H-bonds, or H-bonds involving a C−N-D angle of more than 120°, induce a blue shift in the CN stretch of $SeCN^-$ in D_2O.[28] The formation of axial H-bonds between SCN^- and silanol groups on the pore surface may be responsible for the observed blue shift in the silica pores.

As discussed in the SI, section E, monitoring the time-dependent areas of the MeSCN and SCN^- nitrile stretch bands provides the time-dependent concentrations of these species. The normalized, time-dependent spectra of MeSCN and SCN^- at 296.2 K in bulk MeIm and MeIm confined in the 2.8 nm silica pore are plotted in Figure 3a,b, respectively. The SCN^- spectra are normalized to the peak of the long time spectrum. The MeSCN spectra are normalized to the peak of the earliest spectrum shown in the figure. The insets show an expanded view of the growth of the SCN^- data at relatively short times (hours). Note the scale difference on the insets' vertical axes. As the reaction proceeds, the MeSCN peak area decreases while the SCN^- peak area increases. At very long time, the MeSCN peak completely disappears and the SCN^- peak reaches a maximum, indicating that the reaction has gone to completion. Comparison of Figure 3a,b shows that the SCN^- absorption grows more rapidly when the reaction mixture is confined in silica pores, demonstrating that the reaction rate is accelerated in the pore relative to bulk solution.

3.2. Rate Constant: Temperature Influence. The time-dependent fractional yields of SCN^- in the bulk reaction mixture (Figure 4a) and confined in 2.8 nm pores (Figure 4b) are shown as a function of temperature in Figure 4. At room temperature, the reaction is slow in both systems; the yield is just below 3% in 16 h. However, at elevated temperature the reaction proceeds much faster, and a yield of up to 90% is obtained at 356.2 K in the same time.

As discussed in the SI, section E, the growth of $[SCN^-]$ can be approximated as linear at short time. Linear fits to the data at early time are displayed in Figure 4a,b. The rate constants, k, obtained from the slope of the lines, are listed in Table 3. The bulk rate constant at 336.2 K increases 33-fold relative to that at 296.2 K, consistent with the ~25-fold rate constant enhancement of imidazolium-based ionic liquid Menshutkin reactions with a temperature increase from 298.2 to 333.2 K.[32] At the highest temperature studied, 356.2 K, the rate constants in the bulk and pore increase 127- and 89-fold, respectively,

Table 2. FT IR Line Shape Parameters

	center (cm^{-1})		fwhm[a] (cm^{-1})	
sample	MeSCN	SCN^-	MeSCN	SCN^-
bulk	2154.3 ± 0.1	2054.9 ± 0.1	9.9 ± 0.1	15.4 ± 0.1
8.3 nm	2154.1 ± 0.1	2055.7 ± 0.1	10.3 ± 0.2	15.4 ± 0.1
4.2 nm	2154.3 ± 0.1	2055.8 ± 0.3	10.4 ± 0.3	15.4 ± 0.2
2.8 nm	2154.2 ± 0.1	2055.5 ± 0.2	10.4 ± 0.1	15.4 ± 0.2
2.3 nm MCM41-Si(Me)$_3$	2154.5 ± 0.1	2055.3 ± 0.1	10.7 ± 0.2	15.8 ± 0.3

[a]fwhm: full width at half-maximum.

https://dx.doi.org/10.1021/jacs.9b12666
J. Am. Chem. Soc. XXXX, XXX, XXX−XXX

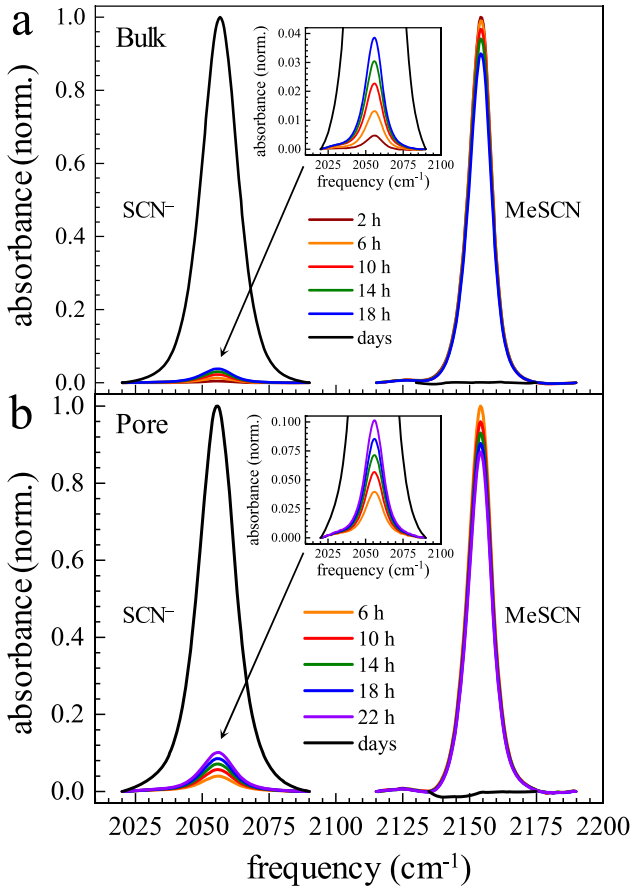

Figure 3. Time-dependent normalized, background subtracted FT IR spectra of MeSCN and SCN^- at 296.2 K in (a) bulk MeIm and (b) in MeIm confined in the 2.8 nm silica pore. The insets show an expanded view of the SCN^- spectra at early reaction times (note different vertical scales).

relative to their values at 296.2 K. Although the relative increase is smaller in the pore system, at each temperature within the investigated range, the pore rate constant is higher than the bulk rate constant. This indicates that the reaction rate is enhanced when confined in the silica pore. The confinement-induced rate constant enhancement increases with decreasing temperature.

The temperature-dependent rate constant for a thermally activated process can be described by the Arrhenius equation

$$k = Ae^{-E_a/RT} \tag{2}$$

where A, E_a, and R are the pre-exponential factor, activation energy, and ideal-gas constant, respectively. The influence of the silica pore on the reaction is further quantified in Figure 4c, which displays a plot of ln k vs $1/T$ (Arrhenius plot). A linear fit to the data yields A and E_a from the intercept and slope, respectively. The activation energies in the pore and bulk systems are 65.9 and 71.4 kJ/mol, respectively, indicating that the pore has a catalytic effect on the reaction. The catalytic function of the pore is analyzed further in sections 3.3 and 3.4 below. The pre-exponential factor also decreases from 7.12×10^9 h^{-1} (bulk) to 1.35×10^9 h^{-1} (pore). Therefore, E_a and A have opposite influences on k in the pore.

The reduction in the pre-exponential factor can be analyzed further by considering Eyring's transition-state theory (TST) expression for the rate constant at fixed pressure[33,34]

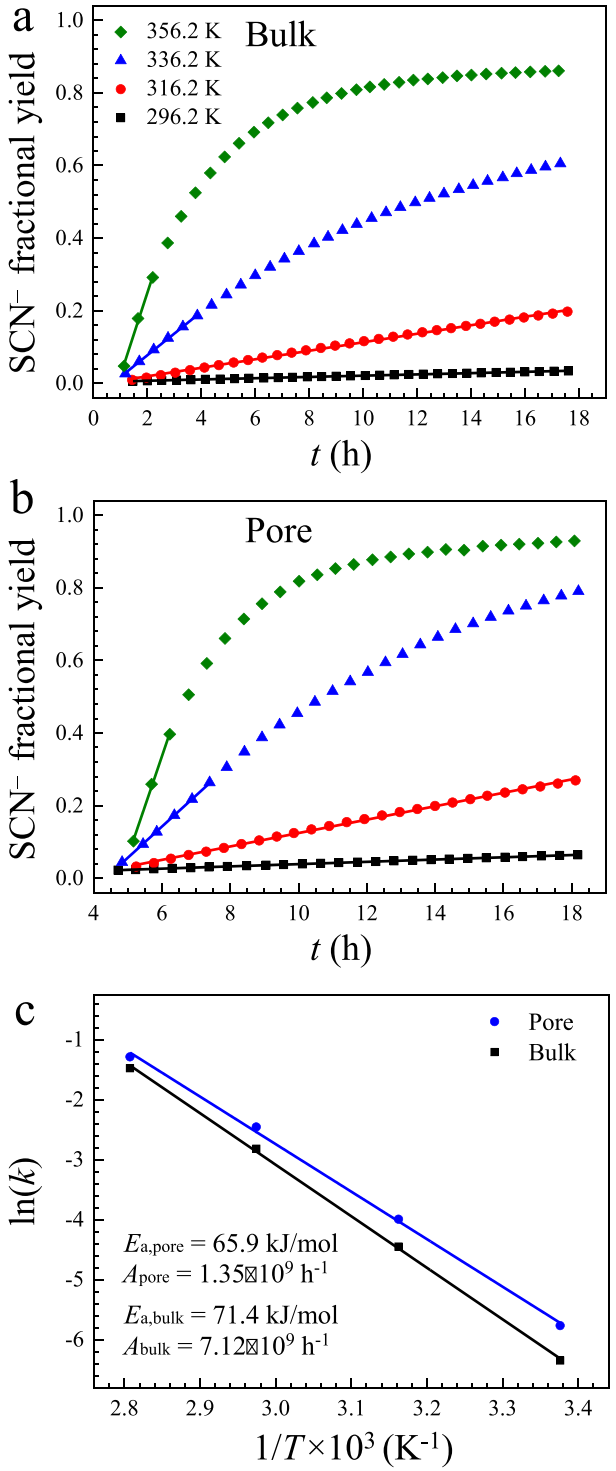

Figure 4. Time-dependent fractional yield of SCN^- in (a) the bulk reaction and (b) the confined reaction in the 2.8 nm silica pore as a function of temperature. (c) Arrhenius plots for the bulk and 2.8 nm pore systems.

$$k_{TST} = \frac{k_B T}{hc^\circ} K^{\ddagger} = \frac{k_B T}{hc^\circ} e^{-\Delta^{\ddagger}G^\circ/RT} \tag{3}$$

where k_B, h, c°, $K^{\ddagger}$, and $\Delta^{\ddagger}G^\circ$ are respectively the Boltzmann constant, Planck's constant, the standard-state concentration (usually 1.00 M), the equilibrium constant between the transition state and reactants, and the standard free energy of

https://dx.doi.org/10.1021/jacs.9b12666
J. Am. Chem. Soc. XXXX, XXX, XXX−XXX

Table 3. Temperature-Dependent Rate Constants in the Bulk and 2.8 nm Pore Systems

	$k \times 10^3$ (h^{-1})			
systems	296.2 K	316.2 K	336.2 K	356.2 K
bulk	1.8	11.7	59.8	228.9
2.8 nm pore	3.1	18.5	85.8	276.3
pore/bulk ratio	1.79	1.58	1.44	1.21

activation. For a bimolecular ideal-gas phase reaction, eq 3 can be written in a form analogous to eq 2[35]

$$k_{TST} = \frac{e^2 k_B T}{hc^\circ} e^{\Delta^\ddagger S^\circ/R} e^{-E_a/RT} \tag{4}$$

where $\Delta^\ddagger S^\circ$ is the standard entropy of activation.

The conventional TST expression cannot account for nonidealities such as high pressure and solvent effects,[1] which are clearly important to the Menshutkin reaction.[10−13] Kramers extended the theory by modeling a chemical reaction as a classical particle of mass, m, moving in a one-dimensional asymmetric double-well potential $U(x)$.[34,36] The remaining degrees of freedom of the surrounding molecules were incorporated as a heat bath at temperature T, which influences the reaction coordinate through a fluctuating force $\xi(t)$ (Brownian motion) and a damping force $-m\gamma\dot{x}$, where γ represents a constant damping rate (friction). For moderate-to-strong friction, he obtained the following result for the rate constant:

$$k = \kappa k_{TST} = \frac{(\gamma^2/4 + {\omega_b}^2)^{1/2} - \gamma/2}{\omega_b} k_{TST} \tag{5}$$

where ${\omega_b}^2$ is related to the curvature of the potential at the position of the transition state.[34,36] The term κ is called the transmission coefficient. κ accounts for recrossing of the barrier from products to reactants, which lowers the rate constant. For nonzero γ, κ is always less than unity, showing that k_{TST} is an upper bound on the rate constant.

Combining the results of Eyring and Kramers, the prefactor A can be expressed as

$$A = \left[\frac{(\gamma^2/4 + {\omega_b}^2)^{1/2} - \gamma/2}{\omega_b}\right] \frac{e^2 k_B T}{hc^\circ} e^{\Delta^\ddagger S^\circ/R} \tag{6}$$

Thus, the reduced prefactor in the pore relative to the bulk system can occur by several mechanisms. One possibility is a decrease in $\Delta^\ddagger S^\circ$, which would indicate that the transition state entropy is closer to that of the reactants in the pore than in the bulk (the results of section 3.4 below lend support to this possibility). A decrease in ω_b, which reflects a decrease in the curvature of the potential at the transition state, could also lower the prefactor by making the barrier more difficult to traverse (in general, broader barriers are more difficult to cross by diffusion). However, we propose that the decrease results primarily from a relative increase in the friction, γ. The coefficient γ is a measure of the strength of the interaction between the reaction coordinate and the surrounding medium. It has often been interpreted[37−40] specifically in terms of Stokes drag,[41] which gives $\gamma = 6\pi\eta r/m$, where η and r are the viscosity of the medium and radius of the spherical particle. In this interpretation, the increased friction reflects an increase in the viscosity of the liquid in the pore, which is mainly the MeIm solvent.

We have performed measurements of the rotational dynamics of the MeSCN in bulk and confined MeIm using IR polarization selective pump−probe experiments.[42−44] The rotational dynamics are significantly slowed in the silica pore, which is consistent with previous measurements on the orientational relaxation of selenocyanate ($SeCN^-$) in silica confined D_2O.[28] In that work, the $SeCN^-$ dynamics were bulk-like in the pore center, but exponentially slowed for $SeCN^-$ molecules closer to the pore surface. A distance decomposition of the rotational dynamics of MeSCN calculated in the model silica pores also shows gradual slowing of the dynamics as the molecule approaches the surface. The Stokes−Einstein−Debye relation for rotational diffusion predicts a direct relationship between the rotational correlation time and the viscosity, or $\tau_R \propto \eta$. Therefore, a confinement induced "effective viscosity" increase would also explain the reduction of the Arrhenius pre-exponential factor in the pore. Indeed, Kramers demonstrated that in the strong friction limit of eq 5, $k \propto \gamma^{-1}$,[36] which based upon the above arguments gives $A \propto \eta^{-1} \propto {\tau_R}^{-1}$. This result has been shown to successfully predict the viscosity dependence of biomolecule folding rates[37−39] and the transition rates of dielectric particles in double-well optical traps.[40,45]

3.3. Rate Constant: Pore-Size Dependence. The reaction rate enhancement in the pore was further investigated by measuring the formation of the SCN^- product as a function of the pore size (Figure 5a). In Figure 5b, the observed k (black points) are plotted as a function of the reciprocal pore radius ($1/R_p$). The data are shown in Table 4. The rate constant increases with $1/R_p$, i.e., decreasing pore size. As the pore size increases, k approaches its bulk value. An increase in the rate constant with decreasing pore size was also observed for the acetalization of cyclohexanone with methanol in MCM41.[19] However, a key difference between this work and previous studies is that here the reaction mixture has been removed from the exterior of the pores (section 2 and SI, section C). Thus, the observed signals originate only from the reactants and products in the silica pore, providing a direct probe of the kinetics occurring in the confined volume.

The measured rate constant represents an ensemble averaged quantity. The spatial variation of the rate constant in the pore can be considered to quantitatively model the size-dependence of k. We tested the ability of the two-state, or core−shell, model[28,46−48] to reproduce the data. The two-state model has found success in describing the behavior of certain molecular properties subject to confinement.[28,46,47,49] For example, in reverse micelle lamellar structures, it has been demonstrated that the water dynamics and FT-IR spectra of the hydroxyl stretch divide into a surface layer one water molecule thick, the shell, and water molecules not at the surface, the core.[47,49] The silica pores studied in this work have approximate cylindrical symmetry. Therefore, the dependence of the property of interest on distance from the pore center, r, provides a complete description of the system. We assume that the rate constant takes on a value in the interfacial, or shell, layer, k_s, and another value in the core region of the pore, k_b. k_b is taken to have the value observed in the bulk reaction mixture. For a pore of radius R_p and shell thickness Δ, $k(r)$ is given by

$$k(r) = k_b + (k_s - k_b)\theta(r - (R_p - \Delta)) \tag{7}$$

where $\theta(x)$ is the Heaviside step function. The spatially averaged rate constant, $k(R_p)$, is calculated by integrating $k(r)$

https://dx.doi.org/10.1021/jacs.9b12666
J. Am. Chem. Soc. XXXX, XXX, XXX−XXX

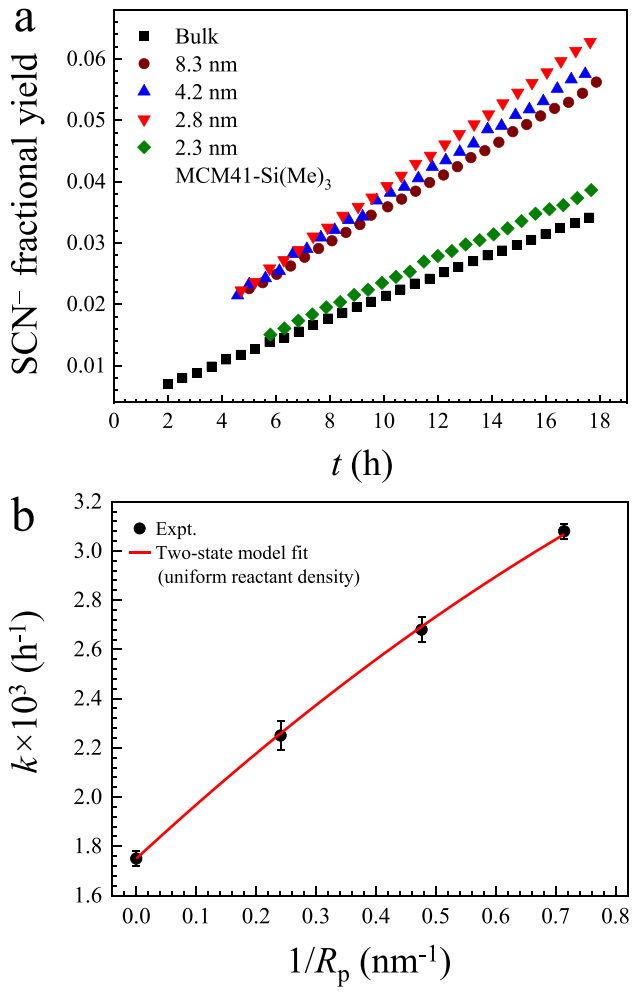

Figure 5. (a) Time-dependent fractional yield of SCN^- in the 2.8 (red points), 4.2 (blue points), and 8.3 nm (brown points) pores at 296.2 K. The data for the reaction in the bulk (black points) and passivated silica pore (green points) are also shown. (b) Measured (black points) and calculated (red curve) rate constants from the two-state model, assuming a uniform reactant density throughout the pore and an interfacial width of Δ = 5.02 Å, as a function of reciprocal pore radius ($1/R_p$) at 296.2 K.

Table 4. Rate Constants in the Bulk and Pore Systems at 296.2 K

systems	$k \times 10^3$ (h^{-1})
bulk	1.8
8.3 nm	2.3
4.2 nm	2.7
2.8 nm	3.1
2.3 nm MCM41-Si(Me)$_3$	1.9

weighted by the probability of finding the reactants between r and $r + dr$, $f(r)dr$, over the entire pore:

$$k(R_p) = \int_0^{R_p} k(r)f(r)dr = k_b + (k_s - k_b)\int_{R_p-\Delta}^{R_p} f(r)dr \quad (8)$$

where $f(r)$ is the probability density function for the reactants. If the reactant density is uniform throughout the pore, $f(r)$ is given by

$$f(r) = \frac{r\int_0^{2\pi} d\theta}{\int_0^{2\pi} d\theta \int_0^{R_p} r dr} = \frac{2r}{R_p{}^2} \quad (9)$$

and, using eq 8, the conventional two-state expression for the rate constant is

$$k(R_p) = k_b + (k_s - k_b)\left\{\frac{2\Delta}{R_p} - \frac{\Delta^2}{R_p{}^2}\right\} \quad (10)$$

As a rough approximation, we first modeled the shell thickness, Δ, as the diameter of one MeIm molecule treated as a perfect sphere. The MeIm volume was calculated to be 66.2 Å^3 using the Connolly volume computation method with a probe radius of zero.[50] Treating MeIm as a sphere, this gives a diameter of D = 5.02 Å. The fit of eq 10 (red curve) to the measured rate constants (black points) using Δ= 5.02 Å and k_b = 1.8 × 10^{-3} h^{-1}, is shown in Figure 5b. Despite this rather crude estimate of the interfacial thickness, Δ, the fit is a reasonable description of the trend of increasing reaction rate with decreasing pore size. A slight curvature is evident in the both the data and fit in Figure 5b. This nonlinear dependence on $1/R_p$ is represented by the second term in brackets in eq 10. The nonlinearity, and therefore curvature of the fit, increases as the interfacial thickness becomes a larger fraction of the pore radii investigated. The only parameter allowed to vary in the fit was the surface rate constant, k_s, which was found to be 4.0 × 10^{-3} h^{-1}. Therefore, the model suggests that molecules within 5 Å of the silica surface react approximately twice as fast as molecules in the core of the silica pores.

Although it is a useful conceptual framework, the conventional two-state model is unrealistic in its treatment of the confined liquid as a continuum with uniform density. The model treats the ratio of the shell area to the total pore cross-sectional area as equivalent to the ratio of the molecules in the shell to the total number of molecules. This ratio of the shell area to the total area is the term in brackets in eq 10. However, the equivalency between the ratio of the areas to the ratio of the number of molecules breaks down when the density of the reactants is not uniform throughout the pores. In this case, the relevant quantity of interest, the ratio of shell molecules to total molecules, is given in general by the final integral in eq 8. In order to compute this integral, the probability density $f(r)$ must be determined.

Molecular dynamics (MD) simulations of the silica pores and reactants were performed to compute $f(r)$. The construction of the silica pore models, the nature of the surface, the pore filling procedure, the force fields and charges, and comparisons to experimental results are discussed in detail in the SI. The simulated probability densities for the C1 and C2 atoms of MeSCN and MeIm (see Figure 1a), respectively, are shown in Figure 6a–c for the 8.3, 4.2, and 2.8 nm pores. The distributions are plotted as a function of the minimum distance between the C atoms and nearest pore O atom, d. The relationship between r and d is given by $R_p = r + d$. The probability densities are peaked at distances close to the pore surface, indicating that the densities of the reactants are nonuniform near the interface (Figure 6). Note that although $f(d)$ appears similar to a radial distribution function (rdf), it is a different quantity. In contrast to an rdf, the integral of $f(d)$ is one by definition. Also, whereas an rdf approaches a value of one as the distance becomes very large (indicating a uniform liquid density), $f(d)$ goes to zero as the pore center is

https://dx.doi.org/10.1021/jacs.9b12666
J. Am. Chem. Soc. XXXX, XXX, XXX−XXX

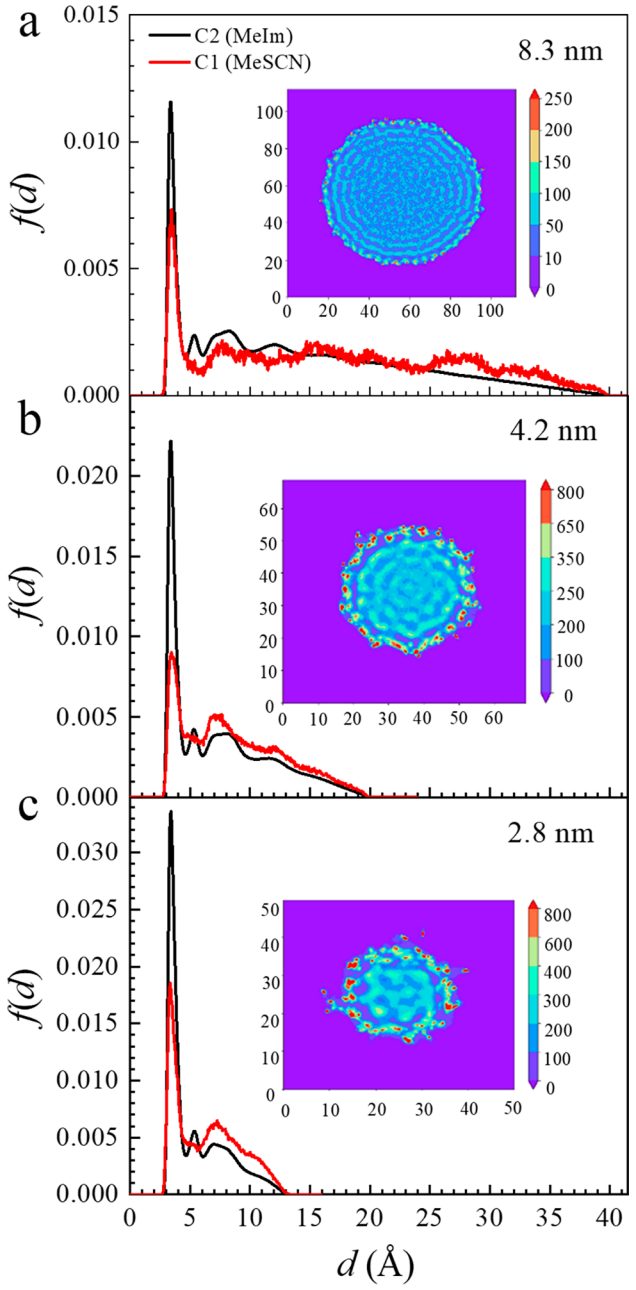

Figure 6. Probability density functions of the MeIm C2 atom and MeSCN C1 atom in the (a) 8.3, (b) 4.2, and (c) 2.8 nm pores as a function of the distance, d, between the C atom and nearest pore O atom. Snapshots of the 2D probability distribution of the MeIm center of mass in the pores are displayed as insets. The inset axes are in angstrom units.

approached and the available volume goes to zero. It can also be seen that $f(d)$ linearly decreases for large d, which reflects a uniform density and linearly decreasing layer volume as the center is approached (analogous to eq 9). The insets to Figure 6a–c display 2D contour plots of the MeIm center of mass positions in the different silica pore models in the xy-plane. The MeIm surface layering is evident for all pore sizes. The layering gradually disappears as d increases, particularly in the 8.3 nm pore where four distinct MeIm layers are discernible followed by unstructured liquid in the pore interior. Four layers are also observed in the 4.2 nm pore; however, the bulk-like liquid in the core region is almost absent. In the 2.8 nm pore, no uniform liquid exists in the core. Similar structural features have been observed for water and ionic liquids confined in porous silica.[28,51−55]

The interfacial thickness, Δ, can be more precisely defined using the probability densities in Figure 6. The first minimum in $f(d)$ arises from the location in between the first and second layers of molecules where the density is lowest. We therefore define the width of the shell to be the distance from d = 0 to the first minimum in $f(d)$ for the MeIm C2 atom. The location of the first minimum is insensitive to the pore size (Figure 6a–c), giving a value of Δ = 4.6 Å for all pores. This value is only about 0.4 Å smaller than the value obtained by treating MeIm as a sphere and taking its diameter, as discussed above. The integral of $f(r)$ over the interfacial region is the ratio of shell molecules to the total number of molecules, which is the quantity needed to model the pore-size dependent rate constants. Using this value of Δ and the $f(r)$ shown in Figure 6a–c, we numerically integrated eq 8 in a global fit to the measured rate constants, with k_s being the single adjustable parameter. The measured rate constants (black points) and calculated rate constants (red points) are shown in Figure 7.

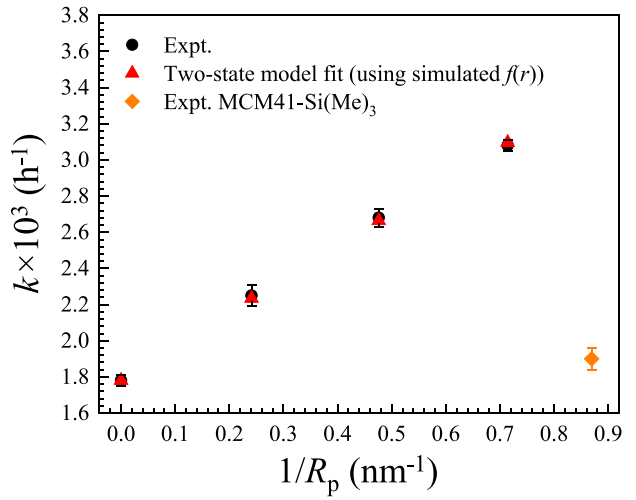

Figure 7. Measured (black points) and calculated (red points) rate constants from the two-state model, using the probability densities in Figure 6, which yield an interfacial width of Δ = 4.6 Å, as a function of reciprocal pore radius ($1/R_p$) at 296.2 K. The measured rate constant in passivated MCM41-Si(Me)$_3$ (orange point, lower right) is also shown for comparison.

The agreement is excellent. This procedure yields k_s = 4.36 × 10^{-3} h^{-1}. This result for k_s is only 7% larger than the result obtained by fitting the data to the two-state model of eq 10, using Δ = 5.02 Å.

The surface rate constant, k_s (4.36 × 10^{-3} h^{-1}), is ∼2.4 times larger than the bulk rate constant, k_b (1.8 × 10^{-3} h^{-1}). It is interesting to note that at 296.2 K, a ratio of $k(R_p = 2.8\ nm)/k_b$ = 9.5 instead of 1.8 is obtained if the pre-exponential factor is assumed to be constant and solely the activation energy change between the bulk and the pore (Figure 4c) is considered. Therefore, the reduction in the pre-exponential factor, A, in the pore relative to the bulk plays a significant role in reducing the magnitude of the rate constant enhancement. As discussed in section 3.2, the decrease in A is correlated with the slowing of MeSCN rotational dynamics observed upon confinement in the 2.8 nm pore. The observations are consistent with similar experiments on the dynamics of $SeCN^-$ in D_2O confined in a

https://dx.doi.org/10.1021/jacs.9b12666
J. Am. Chem. Soc. XXXX, XXX, XXX−XXX

2.4 nm silica pore.[28] Relative to the spatially averaged dynamics, the $SeCN^-$ dynamics near the silica surface were remarkably slower. This is almost certainly the case for confined MeSCN and MeIm. Therefore, A near the pore surface is expected to be smaller than the average value determined in section 3.2 for the 2.8 nm pore. If the surface prefactor is smallest and the rate constant is highest near the surface, the activation energy for the reaction at the surface should be lower than the overall 65.9 kJ/mol value observed experimentally. It is possible to obtain an estimate for both the surface activation energy, $E_{a,s}$ and surface prefactor, A_s. Expressing k_s at two temperature points using eq 2 and taking the ratio of the two equations provides an expression for the surface activation energy, $E_{a,s}$

$$E_{a,s} = \frac{R_p T_1 T_2}{(T_2 - T_1)} \ln\left[\frac{k_s(T_2)}{k_s(T_1)}\right] = \frac{R_p T_1 T_2}{(T_2 - T_1)} \ln\left[\frac{k(T_2) - (1 - \chi_s)k_b(T_2)}{\chi_s k_s(T_1)}\right] \quad (11)$$

where $\chi_s = \int_{R_p - \Delta}^{R_p} f(r)\, dr$. The final form of eq 11 was obtained by using eq 8 to write $k_s(T_2)$ in terms of the pore and bulk rate constants, $k(T_2)$ and $k_b(T_2)$. To obtain $E_{a,s}$, T_1 and $k_s(T_1)$ were fixed to 296.2 K and 4.36×10^{-3} h^{-1}, respectively. The values of the pore rate constant, $k(T_2)$, and the bulk rate constant, $k_b(T_2)$, were measured at three additional T_2 temperatures 316.2, 336.2, and 356.2 K (Table 3). In principle, only two temperature points, T_1 and T_2, are needed to compute $E_{a,s}$. However, to improve the reliability of the calculation, all T_2 points were taken into account by varying $E_{a,s}$, in the least-squares sense, to obtain the best agreement with the three $E_{a,s}$ values predicted from the three temperature points. The result is $E_{a,s} = 64.3 \pm 0.5$ kJ/mol. Using eq 2 and $k_s = 4.4 \times 10^{-3}$ h^{-1} gives $A_s = 9.4 \times 10^8$ h^{-1}. As expected, both the activation energy and prefactor at the silica surface are lower than the same quantities averaged over the entire pore volume.

The above analysis demonstrates that the increased rate constant in the pore can be attributed to a surface-localized enhancement of the reaction rate. Solvent effects are known to have a substantial influence on the rate of Menshutkin reactions.[10,13] In particular, polar solvents can stabilize the charge separation that occurs in the transition state structure.[10,13] These considerations suggest that the solvent structures at the silica surface can stabilize the transition state. The polar, H-bond donating silanols (SiOH) at the surface are likely a key component of these structures.[21] The silanol densities on the surfaces of MCM41 and SBA15 are typically in the range ~2−3 OH groups/nm^2,[56] somewhat lower than the maximum density of ~4.6 OH groups/nm^2 for a fully hydroxylated surface.[57,58] To test the role of the surface silanols in the rate constant enhancement, we measured the rate constant in passivated 2.8 nm MCM41 (MCM41-$Si(Me)_3$) at 296.2 K (Figure 5a, green points), which is shown in Figure 7 (orange point, lower right corner). The rate constant is 1.9×10^{-3} h^{-1} (Figure 7), which is significantly lower than that in the unpassivated MCM41 (3.1×10^{-3} h^{-1}) and nearly identical to the bulk rate constant of 1.8×10^{-3} h^{-1} at the same temperature. We note that the passivation reduces the effective pore diameter from 2.8 to 2.3 nm (Table 1), and a reduction in the pore size is normally associated with an increase in k (Figures 5 and 7). Therefore, the results implicate the silanols in the rate constant enhancement. Both reactants, MeIm and MeSCN, can accept H-bonds from the silanol groups through their σ (nitrogen lone pair) and π orbitals.[30,59,60] The formation of H-bonds between the reactants and surface silanols is responsible for the increased layering of the reactants at the surface as observed in Figure 6a−c. The increased local concentration of reactants at the surface may contribute to the reaction rate enhancement. Additionally, the intermolecular interactions at the surface can orient MeIm and MeSCN preferentially for an S_N2 substitution reaction and stabilize the separation of charge. This possibility is explored in the following section.

3.4. Reaction Energy Profile. To further examine the catalytic effect of the silica surface on the MeIm/MeSCN reaction, density functional theory (DFT) calculations of the reaction energy profile for the hypothetical gas phase reaction were compared to those for the reaction on a SiO_2 surface model without surrounding solvent.[61] This approach is similar to that of Halls and Schlegel,[5] Giacinto et al.,[15] and Tavares et al.[8] The authors used DFT methods to compare the reaction energy profile of the gas phase Menshutkin reaction between ammonia (NH_3) and methyl chloride (CH_3Cl) to that of the same reaction confined in CNTs. Their analyses focused on the relative energies of stationary points on the potential energy surface referred to as the reactant binding complex (CR), transition state (TS), and product binding complex (CP). The authors found activation energies, or the energy difference between the TS and CR (ΔE^*), in the range of ~137−148 kJ/mol for the gas phase reaction. When confined in various types of CNT structures, the activation energies decreased on average by ~40−50 kJ/mol with respect to those in the gas phase reaction.[5,8,15]

In the present work, the results of the rate constant measurements gave a smaller activation energy of 71.4 kJ/mol for the bulk reaction and an activation energy reduction upon confinement in the 2.8 nm silica pore of 5.6 kJ/mol. It is not surprising that the calculated gas phase energies are significantly higher than those observed experimentally given the exclusion of the solvent, which adds a significant degree of stabilization.[62] The comparison is not perfect since both the Menshutkin reaction and confining material investigated here are different from that studied by the above authors. However, given the computational expense, we also adopt the procedure used by these authors. Details on the silica surface model and electronic structure calculations are presented in the SI.

The local surface structures on silica are complicated to model due to surface roughness and the presence of several types of surface silanol groups with different properties.[63,64] Individual silanol groups are classified as "H-bonded" or "isolated" depending on whether they do or do not form H-bonds with other silanols. If two silanols share a common oxygen vertex, they are referred to as "vicinal". "Geminal" silanols have an Si atom that is coordinated to two OH groups. The SiO_2 model (SiO_2-3 with 4.6 OH per nm^2)[61] used here features all of these silanol types.

The Menshutkin reaction proceeds through an S_N2 mechanism in which the nucleophilic N2 of MeIm backside attacks the electrophilic C1 atom of MeSCN (Figure 1a). We hypothesize that MeSCN adsorbs onto the silica surface with its methyl group pointing away from the surface, situating the methyl for effective backside attack. This likely occurs through the formation of an H-bond between the CN group and a silanol OH. Thus, the most stable MeSCN configuration on

https://dx.doi.org/10.1021/jacs.9b12666
J. Am. Chem. Soc. XXXX, XXX, XXX−XXX

the surface was obtained before the transition state calculation was performed. Various adsorption configurations, including their energies, are shown in Figure 8. H-bonds form between the OH groups and the N or S atom of MeSCN in all cases (Figure 8). The adsorption energies are negative, indicating that the H-bond interactions are stabilizing and favor the adsorption. In Figure 8c−e, the CN bond is oriented roughly normal to the surface. For this orientation, the energy is most negative when the CN bond is located near a vicinal silanol (Figure 8c) and becomes progressively more positive in the order geminal (Figure 8d) to isolated (Figure 8e). The large negative energy in the vicinal case results from the added adsorption stabilization offered by the donation of two H-bonds to MeSCN from the two silanols. Figure 8a,b displays MeSCN configurations near vicinal sites in which the CN bond is oriented roughly parallel to the surface. The configuration where the SCN group is nearly flat and the silanol density is highest has the most negative adsorption energy (Figure 8b). In total, three H-bonds between the OH groups on the surface and the N atom (and S atom) are obtained. This configuration was used in the transition state calculation.

The back-side substitution pathway was chosen in the calculation; steric repulsion arising from the interaction between the nucleophile and the leaving group in the front-side pathway renders it highly unfavorable in most cases.[65] Optimized CR, TS, and CP structures in the gas phase and the SiO_2 surface systems are compared in Figure 9a. The relevant geometric parameters are included in Table S1. Comparison of the calculated configurations for the gas phase and silica surface indicates that the SCN groups are stably adsorbed by the silanol groups on the surface via strong H-bond interactions (Table S1).

The reaction energy profiles are shown in Figure 9b. Note that the CR is the zero energy reference point for both the gas phase and silica surface reaction calculations in the figure. The energy barrier, ΔE^*, is the energy difference between the TS and CR. The reaction energy, ΔE^R, is the energy of the CP with respect to the CR. The calculated ΔE^* in the gas phase is 121.5 kJ/mol. This value is consistent with the ∼137−148 kJ/mol range of ΔE^* obtained for the gas phase reaction between NH_3 and CH_3Cl and the ΔE^* of ∼137 kJ/mol calculated for the gas phase Menshutkin reaction between MeIm and chloroethane to produce the ion pair 1-ethyl-3-methylimidazolium chloride (EmimCl).[62] As discussed above, the calculated ΔE^*s for Menshutkin reactions are generally larger than 100 kJ/mol, which is large when compared to experimental results.[62] In this context, the calculated ΔE^* obtained here is reasonable, and the qualitative trends can be compared to previous calculations. The ΔE^* for the surface reaction (76.0 kJ/mol) is reduced relative to that in the gas phase, in qualitative agreement with the reduced activation energy barrier observed in the 2.8 nm pore relative to the bulk. The calculated gas phase barrier reduction is about 37%.

As discussed above, the transition from a hypothetical gas phase reaction to the reaction in the presence of a surface is expected to significantly overestimate the true barrier reduction because the influence of a solvent is not included in this approach. Indeed, in section 3.3 the experimental activation energy at the surface was found to be 64.3 kJ/mol. When compared to the bulk activation energy of 71.4 kJ/mol, this value represents a 10% reduction. Thus, although the quantitative changes predicted from the DFT gas phase calculations are significantly different, the qualitative trends are consistent with the measurements on the Menshutkin reaction in the bulk liquid and nanoconfined liquid. The calculations

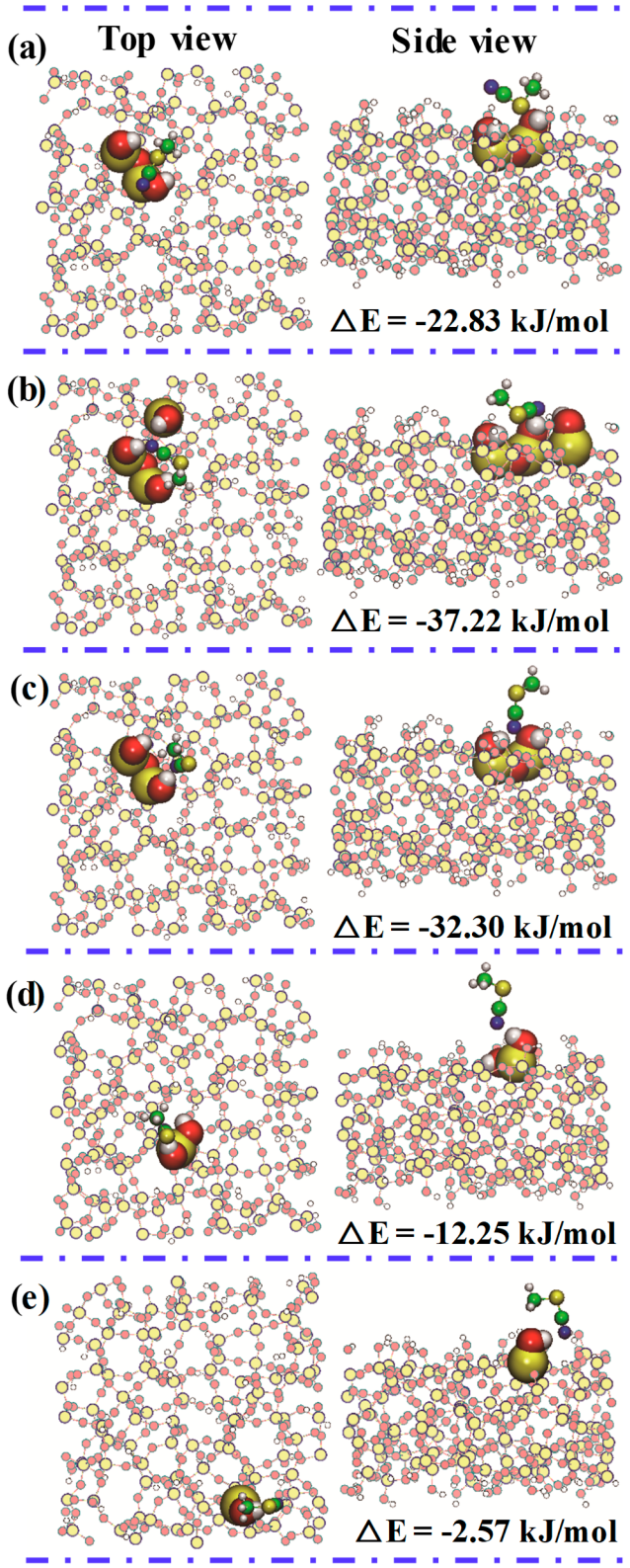

Figure 8. Adsorption configurations and interaction energies for MeSCN close to different types of silanol groups on the silica surface. Panels a−c correspond to vicinal silanols with different MeSCN configurations. Panels d and e show adsorption configurations near geminal and isolated silanols, respectively.

https://dx.doi.org/10.1021/jacs.9b12666
J. Am. Chem. Soc. XXXX, XXX, XXX−XXX

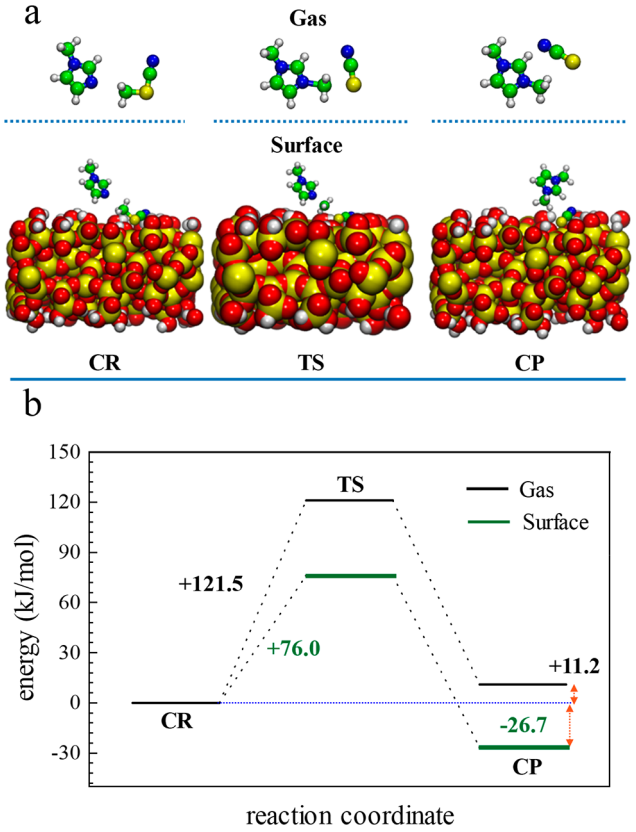

Figure 9. (a) Optimized geometries of reactant binding complexes (CR), transition states (TS), and product binding complexes (CP) and (b) reaction energy profiles for the MeIm/MeSCN reaction in the gas phase and surface systems. The zero energy reference point for both the gas phase and surface systems is the energy of the corresponding CR.

support the conclusion that silanol groups on the surface can act as catalysts by decreasing the reaction energy barrier. In addition, ΔE^R decreases from 11.2 kJ/mol in the gas phase system to −26.7 kJ/mol in the surface system. Therefore, the stabilization of the CP on the surface can reduce the endothermicity of the reaction, in this case, the formerly endothermic reaction becomes exothermic, which was previously calculated for the simplest Menshutkin reaction in CNTs.[8] The reduction in ΔE^R on the silica surface system compared to the gas phase is 37.9 kJ/mol, whereas reductions of around 100 kJ/mol were calculated originally by Halls and Schlegel upon confinement of the reaction in CNTs.[5] However, exothermicity found here is greater than previously reported for CNTs.[8] This is a consequence of the fact that ΔE^R calculated for the gas phase reaction between MeIm and MeSCN is significantly lower than that for NH_3 and CH_3Cl by over 100 kJ/mol,[5,8,15] which is notable given the similar ΔE^* energies obtained. The calculations indicate that the present reaction is more thermodynamically favored compared to the one between NH_3 and CH_3Cl.

4. CONCLUDING REMARKS

The kinetics of the Menshutkin reaction between MeIm and MeSCN confined in mesoporous silica were investigated as a function of temperature, pore size, and surface chemistry using FT IR spectroscopy, MD simulations, and ab initio calculations. Pseudo-first order rate constants were obtained from the growth of the absorption of the CN stretch of the SCN^- product at early time in the bulk and pore systems. The rate constants are larger in the pore systems for all investigated diameters (2.8, 4.2, and 8.3 nm) and temperatures, which is consistent with previous studies.[5,8,19,20]

The temperature dependence of the rate constant in the bulk and the 2.8 nm pore follows an Arrhenius trend. The activation energy for the reaction in the pore is 5.6 kJ/mol lower than in the bulk. The increase in rate constant with decreasing pore size can be quantitatively described by a two-state model,[46,66] in which the pore is partitioned into a shell region with enhanced kinetics and a core region with bulk kinetics. The effectiveness of the two-state model in describing the pore-size dependence of the rate constant indicates that the enhancement is mainly a surface effect that does not change with confinement size. The average rate constant increases with decreasing pore size as molecules in the shell become a larger fraction of the total reacting population. While the reduced surface activation energy ultimately favors the reaction in the shell, the pre-exponential factor, which decreases in tandem with the slower interfacial solvent dynamics, disfavors the reaction. The role of surface silanols in the rate constant enhancement was confirmed by observing the reaction in passivated 2.3 nm MCM41 (MCM41-Si$(Me)_3$), which was only slightly faster than in bulk solution and much slower than in the unpassivated 2.8 nm MCM41. Simulations of the MeIm probability density near the silica surface show that the interfacial layer thickness, Δ = 4.6 Å, is independent of pore size. This value yields a 2.4-fold rate constant increase in the shell relative to the core.

The calculated reactant adsorption energies on the silica surface show that vicinal sites where the SCN group is oriented parallel to the surface are most stable. This configuration increases the number of H-bonds formed between the surface and the MeSCN while orienting the methyl group away from the surface for effective attack by the MeIm nucleophile. Additionally, the H-bonds increase the electrophilicity of the methyl group by directing electron density toward the N terminus of the molecule, increasing the reactivity. These changes are reflected in the reduced activation energy on the silica surface relative to the gas phase. This is consistent with the present experiments and the reduced barrier calculated for the reaction between NH_3 and CH_3Cl confined in a CNT.[5,8] The calculations further show that the silica surface can stabilize the product binding complex, making the formerly endothermic reaction in the gas phase exothermic in the silica pore. This effect is predicted to occur in CNTs as well.[5,8,15]

This work overcomes the existing difficulties associated with selecting, characterizing, and observing Menshutkin reactions in porous host materials. The rate constant trends, kinetic heterogeneity modeling, and mechanistic insights presented here can inform future investigations of nanoconfined reactions and aid in the development of design principles that tailor nanostructured materials for reactions of interest.

■ ASSOCIATED CONTENT

Supporting Information

The Supporting Information is available free of charge at https://pubs.acs.org/doi/10.1021/jacs.9b12666.

Surface areas, pore size distributions, pore volumes, synthesis of MCM41-Si$(Me)_3$, sample preparation and TGA analysis, sample cell assembly and linear IR

https://dx.doi.org/10.1021/jacs.9b12666
J. Am. Chem. Soc. XXXX, XXX, XXX−XXX

spectroscopy, rate constant determination, transition state theory, classical MD simulations, reaction energy profile calculations, Figures S1−S4, and Tables S1 and S2 (PDF)

AUTHOR INFORMATION

Corresponding Authors

Michael D. Fayer − *Department of Chemistry, Stanford University, Stanford, California 94305, United States;* orcid.org/0000-0002-0021-1815; Email: fayer@stanford.edu

Ling Zhao − *State Key Laboratory of Chemical Engineering, East China University of Science and Technology, Shanghai 200237, China;* orcid.org/0000-0001-5239-1152; Email: zhaoling@ecust.edu.cn

Authors

Weizhong Zheng − *Department of Chemistry, Stanford University, Stanford, California 94305, United States; State Key Laboratory of Chemical Engineering, East China University of Science and Technology, Shanghai 200237, China*

Steven A. Yamada − *Department of Chemistry, Stanford University, Stanford, California 94305, United States;* orcid.org/0000-0003-3171-1625

Samantha T. Hung − *Department of Chemistry, Stanford University, Stanford, California 94305, United States*

Weizhen Sun − *State Key Laboratory of Chemical Engineering, East China University of Science and Technology, Shanghai 200237, China;* orcid.org/0000-0002-9957-3620

Complete contact information is available at: https://pubs.acs.org/10.1021/jacs.9b12666

Author Contributions

[§]W.Z. and S.A.Y. contributed equally to this work.

Notes

The authors declare no competing financial interest.

ACKNOWLEDGMENTS

This work was funded by the Division of Chemical Sciences, Geosciences, and Biosciences, Office of Basic Energy Sciences of the U.S. Department of Energy through Grant No. DE-FG03-84ER13251 (W.Z., S.A.Y., and M.D.F.). S.T.H. was supported by the National Science Foundation through the CCI program, CHE-1740645. Part of this work was performed at the Stanford Nano Shared Facilities (SNSF), supported by the National Science Foundation under Award ECCS-1542152. We thank Stanford University and the Stanford Research Computing Center for providing computational resources for this research; the ab initio calculations were performed on the Sherlock cluster at Stanford. The MD simulations were performed on a home-built cluster in China, and we thank Cao Piao, Zhennan Wang, and Xiaohong Liu for their help with the MD simulation data transfer. W.Z. gratefully acknowledges the support from the China Scholarship Council (No. 201806740046) during his work at Stanford University. S.A.Y. gratefully acknowledges the support from a Stanford Graduate Fellowship. We thank Maolin Sha and Boning Wu for their constructive suggestions on the simulation methods and analysis code and Sean Roget for his constructive comments on the manuscript.

REFERENCES

(1) Turner, C. H.; Brennan, J. K.; Johnson, J. K.; Gubbins, K. E. Effect of confinement by porous materials on chemical reaction kinetics. *J. Chem. Phys.* **2002**, *116*, 2138.

(2) Santiso, E. E.; George, A. M.; Turner, C. H.; Kostov, M. K.; Gubbins, K. E.; Buongiorno-Nardelli, M.; Sliwinska-Bartkowiak, M. Adsorption and catalysis: The effect of confinement on chemical reactions. *Appl. Surf. Sci.* **2005**, *252*, 766.

(3) Miners, S. A.; Rance, G. A.; Khlobystov, A. N. Chemical reactions confined within carbon nanotubes. *Chem. Soc. Rev.* **2016**, *45*, 4727.

(4) Solomonsz, W. A.; Rance, G. A.; Harris, B. J.; Khlobystov, A. N. Competitive hydrosilylation in carbon nanoreactors: probing the effect of nanoscale confinement on selectivity. *Nanoscale* **2013**, *5*, 12200.

(5) Halls, M. D.; Schlegel, H. B. Chemistry inside carbon nanotubes: the Menshutkin S_N2 reaction. *J. Phys. Chem. B* **2002**, *106*, 1921.

(6) Halls, M. D.; Raghavachari, K. Carbon Nanotube Inner Phase Chemistry: The Cl^- Exchange S_N2 Reaction. *Nano Lett.* **2005**, *5*, 1861.

(7) Giacinto, P.; Bottoni, A.; Calvaresi, M.; Zerbetto, F. $Cl^{(-)}$ Exchange S_N2 Reaction inside Carbon Nanotubes: C−H···π and Cl···π Interactions Govern the Course of the Reaction. *J. Phys. Chem. C* **2014**, *118*, 5032.

(8) Tavares, I.; Figueiredo, C.; Magalhães, A. The Inner Cavity of a Carbon Nanotube as a Chemical Reactor: Effect of Geometry on the Catalysis of a Menshutkin S_N2 Reaction. *J. Phys. Chem. C* **2017**, *121*, 2165.

(9) Menschutkin, N. Beiträge zur Kenntnis der Affinitätskoeffizienten der Alkylhaloide und der organischen Amine. *Z. Phys. Chem.* **1890**, *5*, 589.

(10) Auriel, M.; de Hoffmann, E. Quantitative study of solvent effects on the Menshutkin reaction between 1,4-diazabicyclo[2.2.2]-octane and 2-chloroethylbenzene, 2-bromoethylbenzene, and 2-iodoethylbenzene. Part 2. Mixed solvents. *J. Chem. Soc., Perkin Trans. 2* **1979**, 325.

(11) Sola, M.; Lledos, A.; Duran, M.; Bertran, J.; Abboud, J. L. M. Analysis of solvent effects on the Menshutkin reaction. *J. Am. Chem. Soc.* **1991**, *113*, 2873.

(12) Abboud, J. L. M.; Notario, R.; Bertran, J.; Sola, M. In *Prog. Phys. Org. Chem.*; Taft, R. W., Ed.; John Wiley & Sons: New York, 1993; Vol. *19*, p 1.

(13) Maran, U.; Pakkanen, T. A.; Karelson, M. Semiempirical study of the solvent effect on the Menshutkin reaction. *J. Chem. Soc., Perkin Trans. 2* **1994**, 2445.

(14) Melo, A.; Alfaia, A. J.; Reis, J. C. R.; Calado, A. R. Unusual Solvent Effect on a SN2 Reaction. A Quantum-Mechanical and Kinetic Study of the Menshutkin Reaction between 2-Amino-1-methylbenzimidazole and Iodomethane in the Gas Phase and in Acetonitrile. *J. Phys. Chem. B* **2006**, *110*, 1877.

(15) Giacinto, P.; Zerbetto, F.; Bottoni, A.; Calvaresi, M. CNT-confinement effects on the Menshutkin S_N2 reaction: the role of nonbonded interactions. *J. Chem. Theory Comput.* **2016**, *12*, 4082.

(16) Liu, C.; Cheng, H.-M. Controlled Growth of Semiconducting and Metallic Single-Wall Carbon Nanotubes. *J. Am. Chem. Soc.* **2016**, *138*, 6690.

(17) Beck, J. S.; Vartuli, J. C.; Roth, W. J.; Leonowicz, M. E.; Kresge, C. T.; Schmitt, K. D.; Chu, C. T. W.; Olson, D. H.; Sheppard, E. W.; McCullen, S. B.; Higgins, J. B.; Schlenker, J. L. A new family of mesoporous molecular sieves prepared with liquid crystal templates. *J. Am. Chem. Soc.* **1992**, *114*, 10834.

(18) Kresge, C. T.; Leonowicz, M. E.; Roth, W. J.; Vartuli, J. C.; Beck, J. S. Ordered mesoporous molecular sieves synthesized by a liquid-crystal template mechanism. *Nature* **1992**, *359*, 710.

(19) Iwamoto, M.; Tanaka, Y.; Sawamura, N.; Namba, S. Remarkable effect of pore size on the catalytic activity of mesoporous silica for the acetalization of cyclohexanone with methanol. *J. Am. Chem. Soc.* **2003**, *125*, 13032.

https://dx.doi.org/10.1021/jacs.9b12666
J. Am. Chem. Soc. XXXX, XXX, XXX−XXX

(20) Xiao, S.; Xu, G.; Chen, G.; Mu, X.; Chen, Z.; Zhu, J.; He, Y. Intramolecular cyclization of N-phenylanthranilic acid catalyzed by MCM-41 with different pore diameters. *Res. Chem. Intermed.* **2015**, *41*, 10125.
(21) Eslami, M.; Dekamin, M. G.; Motlagh, L.; Maleki, A. MCM-41 mesoporous silica: a highly efficient and recoverable catalyst for rapid synthesis of α-aminonitriles and imines. *Green Chem. Lett. Rev.* **2018**, *11*, 36.
(22) García, A.; Slowing, I. I.; Evans, J. W. Pore diameter dependence of catalytic activity: p-nitrobenzaldehyde conversion to an aldol product in amine-functionalized mesoporous silica. *J. Chem. Phys.* **2018**, *149*, No. 024101.
(23) Brunauer, S.; Emmett, P. H.; Teller, E. Adsorption of gases in multimolecular layers. *J. Am. Chem. Soc.* **1938**, *60*, 309.
(24) Barrett, E. P.; Joyner, L. G.; Halenda, P. P. The Determination of Pore Volume and Area Distributions in Porous Substances. I. Computations from Nitrogen Isotherms. *J. Am. Chem. Soc.* **1951**, *73*, 373.
(25) Jaroniec, C. P.; Kruk, M.; Jaroniec, M.; Sayari, A. Tailoring Surface and Structural Properties of MCM-41 Silicas by Bonding Organosilanes. *J. Phys. Chem. B* **1998**, *102*, 5503.
(26) Anwander, R.; Nagl, I.; Widenmeyer, M.; Engelhardt, G.; Groeger, O.; Palm, C.; Röser, T. Surface Characterization and Functionalization of MCM-41 Silicas via Silazane Silylation. *J. Phys. Chem. B* **2000**, *104*, 3532.
(27) Antochshuk, V.; Jaroniec, M. Adsorption, Thermogravimetric, and NMR Studies of FSM-16 Material Functionalized with Alkylmonochlorosilanes. *J. Phys. Chem. B* **1999**, *103*, 6252.
(28) Yamada, S. A.; Shin, J. Y.; Thompson, W. H.; Fayer, M. D. Water Dynamics in Nanoporous Silica: Ultrafast Vibrational Spectroscopy and Molecular Dynamics Simulations. *J. Phys. Chem. C* **2019**, *123*, 5790.
(29) Kittaka, S.; Iwashita, T.; Serizawa, A.; Kranishi, M.; Takahara, S.; Kuroda, Y.; Mori, T.; Yamaguchi, T. Low temperature properties of acetonitrile confined in MCM-41. *J. Phys. Chem. B* **2005**, *109*, 23162.
(30) Shin, J. Y.; Wang, Y.-L.; Yamada, S. A.; Hung, S. T.; Fayer, M. D. Imidazole and 1-Methylimidazole Hydrogen Bonding and Nonhydrogen Bonding Liquid Dynamics: Ultrafast IR Experiments. *J. Phys. Chem. B* **2019**, *123*, 2094.
(31) Morales, C. M.; Thompson, W. H. Simulations of infrared spectra of nanoconfined liquids: Acetonitrile confined in nanoscale, hydrophilic silica pores. *J. Phys. Chem. A* **2009**, *113*, 1922.
(32) Schleicher, J. C.; Scurto, A. M. Kinetics and solvent effects in the synthesis of ionic liquids: imidazolium. *Green Chem.* **2009**, *11*, 694.
(33) Eyring, H. The Activated Complex in Chemical Reactions. *J. Chem. Phys.* **1935**, *3*, 107.
(34) Hänggi, P.; Talkner, P.; Borkovec, M. Reaction-rate theory: fifty years after Kramers. *Rev. Mod. Phys.* **1990**, *62*, 251.
(35) McQuarrie, D. A.; Simon, J. D. *Physical Chemistry: A Molecular Approach*; University Science Books: Sausalito, CA, 1997.
(36) Kramers, H. A. Brownian motion in a field of force and the diffusion model of chemical reactions. *Physica* **1940**, *7*, 284.
(37) Hori, N.; Denesyuk, N. A.; Thirumalai, D. Frictional Effects on RNA Folding: Speed Limit and Kramers Turnover. *J. Phys. Chem. B* **2018**, *122*, 11279.
(38) Klimov, D. K.; Thirumalai, D. Viscosity Dependence of the Folding Rates of Proteins. *Phys. Rev. Lett.* **1997**, *79*, 317.
(39) Stephen, J. H. Solvent Viscosity and Friction in Protein Folding Dynamics. *Curr. Protein Pept. Sci.* **2010**, *11*, 385.
(40) McCann, L. I.; Dykman, M.; Golding, B. Thermally activated transitions in a bistable three-dimensional optical trap. *Nature* **1999**, *402*, 785.
(41) Stokes, G. On the effect of internal friction of fluids on the motion of pendulums. *Trans. Cambridge Philos. Soc.* **1850**, *9*, 106.
(42) Tokmakoff, A. Orientational correlation functions and polarization selectivity for nonlinear spectroscopy of isotropic media. I. Third order. *J. Chem. Phys.* **1996**, *105*, 1.
(43) Tao, T. Time-dependent fluorescence depolarization and Brownian rotational diffusion coefficients of macromolecules. *Biopolymers* **1969**, *8*, 609.
(44) Tan, H.-S.; Piletic, I. R.; Fayer, M. D. Polarization selective spectroscopy experiments: methodology and pitfalls. *J. Opt. Soc. Am. B* **2005**, *22*, 2009.
(45) Rondin, L.; Gieseler, J.; Ricci, F.; Quidant, R.; Dellago, C.; Novotny, L. Direct measurement of Kramers turnover with a levitated nanoparticle. *Nat. Nanotechnol.* **2017**, *12*, 1130.
(46) Thompson, W.; Perspective, H. Dynamics of confined liquids. *J. Chem. Phys.* **2018**, *149*, 170901.
(47) Moilanen, D. E.; Fenn, E. E.; Wong, D.; Fayer, M. D. Water dynamics in large and small reverse micelles: From two ensembles to collective behavior. *J. Chem. Phys.* **2009**, *131*, No. 014704.
(48) Piletic, I. R.; Moilanen, D. E.; Spry, D. B.; Levinger, N. E.; Fayer, M. D. Testing the Core/Shell Model of Nanoconfined Water in Reverse Micelles Using Linear and Nonlinear IR Spectroscopy. *J. Phys. Chem. A* **2006**, *110*, 4985.
(49) Fenn, E. E.; Wong, D. B.; Fayer, M. D. Water dynamics at neutral and ionic interfaces. *Proc. Natl. Acad. Sci. U. S. A.* **2009**, *106*, 15243.
(50) Connolly, M. L. Computation of molecular volume. *J. Am. Chem. Soc.* **1985**, *107*, 1118.
(51) Bonnaud, P. A.; Coasne, B.; Pellenq, R. J. Molecular simulation of water confined in nanoporous silica. *J. Phys.: Condens. Matter* **2010**, *22*, 284110.
(52) Bourg, I. C.; Steefel, C. I. Molecular dynamics simulations of water structure and diffusion in silica nanopores. *J. Phys. Chem. C* **2012**, *116*, 11556.
(53) Mendonça, A. C.; Malfreyt, P.; Pádua, A. A. Interactions and ordering of ionic liquids at a metal surface. *J. Chem. Theory Comput.* **2012**, *8*, 3348.
(54) Singh, M. P.; Singh, R. K.; Chandra, S. Ionic liquids confined in porous matrices: physicochemical properties and applications. *Prog. Mater. Sci.* **2014**, *64*, 73.
(55) Yan, Z.; Meng, D.; Wu, X.; Zhang, X.; Liu, W.; He, K. Two-dimensional ordering of ionic liquids confined by layered silicate plates via molecular dynamics simulation. *J. Phys. Chem. C* **2015**, *119*, 19244.
(56) Zhao, X. S.; Lu, G. Q.; Whittaker, A. K.; Millar, G. J.; Zhu, H. Y. Comprehensive study of surface chemistry of MCM-41 using 29Si CP/MAS NMR, FTIR, pyridine-TPD, and TGA. *J. Phys. Chem. B* **1997**, *101*, 6525.
(57) Zhuravlev, L. Concentration of hydroxyl groups on the surface of amorphous silicas. *Langmuir* **1987**, *3*, 316.
(58) Zhuravlev, L. The surface chemistry of amorphous silica. Zhuravlev model. *Colloids Surf., A* **2000**, *173*, 1.
(59) Maienschein-Cline, M. G.; Londergan, C. H. The CN Stretching Band of Aliphatic Thiocyanate is Sensitive to Solvent Dynamics and Specific Solvation. *J. Phys. Chem. A* **2007**, *111*, 10020.
(60) Oh, K.-I.; Choi, J.-H.; Lee, J.-H.; Han, J.-B.; Lee, H.; Cho, M. Nitrile and thiocyanate IR probes: Molecular dynamics simulation studies. *J. Chem. Phys.* **2008**, *128*, 154504.
(61) Comas-Vives, A. Amorphous SiO_2 surface models: energetics of the dehydroxylation process, strain, ab initio atomistic thermodynamics and IR spectroscopic signatures. *Phys. Chem. Chem. Phys.* **2016**, *18*, 7475.
(62) Mu, X.; Jiang, N.; Liu, C.; Zhang, D. New Insight into the Formation Mechanism of Imidazolium-Based Ionic Liquids from N-Alkyl Imidazoles and Halogenated Hydrocarbons: A Polar Microenvironment Induced and Autopromoted Process. *J. Phys. Chem. A* **2017**, *121*, 1133.
(63) Leung, K.; Nielsen, I. M.; Criscenti, L. J. Elucidating the bimodal acid− base behavior of the water− silica interface from first principles. *J. Am. Chem. Soc.* **2009**, *131*, 18358.
(64) Pfeiffer-Laplaud, M.; Costa, D.; Tielens, F.; Gaigeot, M.-P.; Sulpizi, M. Bimodal acidity at the amorphous silica/water interface. *J. Phys. Chem. C* **2015**, *119*, 27354.

https://dx.doi.org/10.1021/jacs.9b12666
J. Am. Chem. Soc. XXXX, XXX, XXX−XXX

(65) Hamlin, T. A.; Swart, M.; Bickelhaupt, F. M. Nucleophilic Substitution (S_N2): Dependence on Nucleophile, Leaving Group, Central Atom, Substituents, and Solvent. *ChemPhysChem* **2018**, *19*, 1315.
(66) Gulmen, T. S.; Thompson, W. H. Testing a two-state model of nanoconfined liquids: Conformational equilibrium of ethylene glycol in amorphous silica pores. *Langmuir* **2006**, *22*, 10919.

https://dx.doi.org/10.1021/jacs.9b12666
J. Am. Chem. Soc. XXXX, XXX, XXX−XXX